

Revealing the role of organic cations in hybrid halide perovskite $\text{CH}_3\text{NH}_3\text{PbI}_3$

Carlo Motta,^{1,2,*} Fedwa El Mellouhi,^{2,†} Sabre Kais,^{2,3}

Nouar Tabet,² Fahhad Alharbi,² and Stefano Sanvito¹

¹*School of Physics, AMBER and CRANN Institute, Trinity College, Dublin 2, Ireland*

²*Qatar Environment and Energy Research Institute, P.O. Box 5825 Doha, Qatar*

³*Department of Chemistry and Physics, Purdue University, USA*

(Dated: January 16, 2015)

Abstract

The hybrid halide perovskite $\text{CH}_3\text{NH}_3\text{PbI}_3$ has enabled solar cells to reach an efficiency of about 18%, demonstrating a pace for improvements with no precedents in the solar energy arena. Despite such explosive progress, the microscopic origin behind the success of such material is still debated, with the role played by the organic cations in the light-harvesting process remaining unclear. Here van-der-Waals-corrected density functional theory calculations reveal that the orientation of the organic molecules plays a fundamental role in determining the material electronic properties. For instance, if CH_3NH_3 orients along a (011)-like direction, the PbI_6 octahedral cage will distort and the band gap will become indirect. Our results suggest that molecular rotations, with the consequent dynamical change of the band structure, might be at the origin of the slow carrier recombination and the superior conversion efficiency of $\text{CH}_3\text{NH}_3\text{PbI}_3$.

INTRODUCTION

Very few materials have taken a research field by storm as the hybrid halide perovskites have done in the last two years in the solar cell community¹. These are compounds with the standard AMX_3 perovskite structure, where X is the halide iodine, M is lead, while the remaining cation position, A, is taken by an organic molecule, in this case methylammonium, CH_3NH_3 . The success of such compounds is that high-efficiency solar cells can be fabricated cheaply from the liquid phase^{2,3} and that the efficiency can be tuned by controlling their structural order and composition^{4,5}. Particularly intriguing is the fact that high efficiencies are achieved even for planar cells⁶, indicating that charge separation can occur in the hybrid perovskite absorber and that efficient charge diffusion takes place for both electrons and holes⁷.

Part of this behaviour can be related to the unusual situation concerning possible intrinsic defects. Recent electronic structure calculations^{8,9} have shown that the dominant simple or complex defects in $CH_3NH_3PbI_3$ produce only shallow defect levels, while those able to act as deep traps have a high formation energy. Such observation suggests that, under ideal conditions, deep-level point defects cannot act as non-radiative recombination sites; a fact that can partially explain the relative long exciton lifetimes and diffusion lengths observed in these materials. At the same time the absence of deep levels may explain also the large open-circuit voltage measured. However, despite all these hints many fundamental questions remain open. In particular it is still not clear what is the role played by the organic molecules in the efficiency of these compounds. Theoretical investigations have now built a consensus that the methylammonium (MA) group does not have any significant contribution to the electronic structure around the band edges^{8,10,11} and suggest that the only role of the molecules is that of donating an electron to the Pb-I framework, thus stabilizing the perovskite structure.

Interestingly, not even the geometrical arrangement of the MA group is known in detail. At low temperature (below 150 K) the crystal adopts an orthorhombic ($Pnma$) structure, in which the PbI_6 octahedra are strongly deformed assuming a rectangular basal plane. Such deformation restricts the rotational degrees of freedom of MA in the rhombus-shaped interstitial region, thus imposing a spatial ordering to CH_3NH_3 . In this case the organic cation is pinned and can only rotate along the C-N axis. As the temperature is increased

and the material progressively assumes a cubic structure ($Pm-3m$), by passing through a tetragonal one ($I4/m$), the CH_3NH_3 molecules become free to rotate between the octahedral cages. Above room temperature such rotation is fast, to a point where both crystallographic analysis^{3,12} and NMR measurements¹³ have shown that the exact location of the MA groups cannot be determined.

Here we conduct density functional theory (DFT) calculations for $\text{CH}_3\text{NH}_3\text{PbI}_3$ in the cubic phase, by taking into consideration the experimentally reported evidence of the fast rotation of CH_3NH_3 . This means that we do not limit our analysis to CH_3NH_3 oriented along the (100) or (111) direction, for which the high O_h symmetry is maintained, but we also explore cases where the symmetry is lowered. We find that such symmetry lowering has profound consequences on the electronic structure, namely that the bandgap changes from direct to indirect. Crucially such symmetry-lowering configurations represent local minima in the free energy surface of the crystal and they are stabilized by van der Waals (vdW) interactions. These are the key ingredient not only for obtaining accurate lattice parameters^{12,14-17} (see Supplementary Figure 1) but also for the internal geometry. Our calculations then return a picture of the $\text{CH}_3\text{NH}_3\text{PbI}_3$ as a “dynamical” bandgap semiconductor, in which the exact position of the conduction band minimum depends on the particular spatial arrangement of the molecules. Importantly our results are robust against bandgap corrections and spin-orbit interaction^{11,18-21}, and deliver an absorption spectrum in good agreement with experimental data near the absorption edge.^{7,22}

RESULTS

Geometrical Optimization

Let us start the discussion by presenting the relaxed crystal geometries. Initially all the calculations have been performed at the level of the generalized gradient approximation (GGA)²³ to the DFT exchange and correlation functional, including vdW interactions²⁴ (see computational details section) and without explicitly considering spin-orbit coupling (SOC). Additional calculations beyond the GGA and including SOC will be discussed later in relation to the electronic structure.

In Fig. 1 the relaxed structures for the cubic phase of $\text{CH}_3\text{NH}_3\text{PbI}_3$ are presented along

the xy and xz planes for two different orientations of the CH_3NH_3 cation. The relaxation process is extremely sensitive to the initial conditions. When we start the geometrical optimization with the molecular cation oriented along the (111) direction, the structure relaxes maintaining the same orientation [panel (a)]. In contrast, by starting from a (001) oriented molecule the relaxation may end up with CH_3NH_3 along (011) [panel (b)] or an equivalent directions. However, it is important to point out that the cation energy landscape is very shallow. Indeed, both configurations represent local energy minima, with an energy difference of only about 20 meV in favor of (011). In both cases, the lattice parameter is calculated in excellent agreement with the experimental value of 6.329\AA ²⁵ and an error of less than 0.8% (see Supplementary Table 1 and Supplementary Figure 1). If one does not include vdW forces in the relaxation, the discrepancy with the nominal value will become larger than 2%, i.e. the crystal structure is not properly described. Furthermore, the molecular bending angle increases from 16° to 25° upon inclusion of dispersion forces. In order to make a well-grounded comparison with previous calculations^{11,26} reporting no effect of methylammonium on the structure, we started the relaxation from the experimentally published atomic coordinates with CH_3NH_3 along (100)²⁷, whose band structure is presented in Supplementary Figure 2.

By inspecting the relaxed structures a prominent difference between the (111) and the other two geometries appears. In fact, in the case of (011) the rotation of the cation induces a deformation and a symmetry reduction of the inorganic PbI_6 octahedra. The result of such PbI_6 octahedra distortion is that the Pb-I bonds do not lie parallel to the crystal directions, but instead they slightly deviate by approximately 6° . Unlike the (111) case, the unit cell becomes pseudocubic with the lattice parameters along the y and z directions being 1% larger than that along x . Hence, it is clear that the dispersive forces are critical for the internal geometry optimization and consequently, as we will see next, for the electronic behavior of hybrid perovskites.

Electronic Properties

The fine differences in the crystal geometries have a qualitatively strong impact on the electronic structure. In Fig. 2 we show the electronic bandstructure along some high symmetry points of the Brillouin zone calculated with and without including SOC. For both

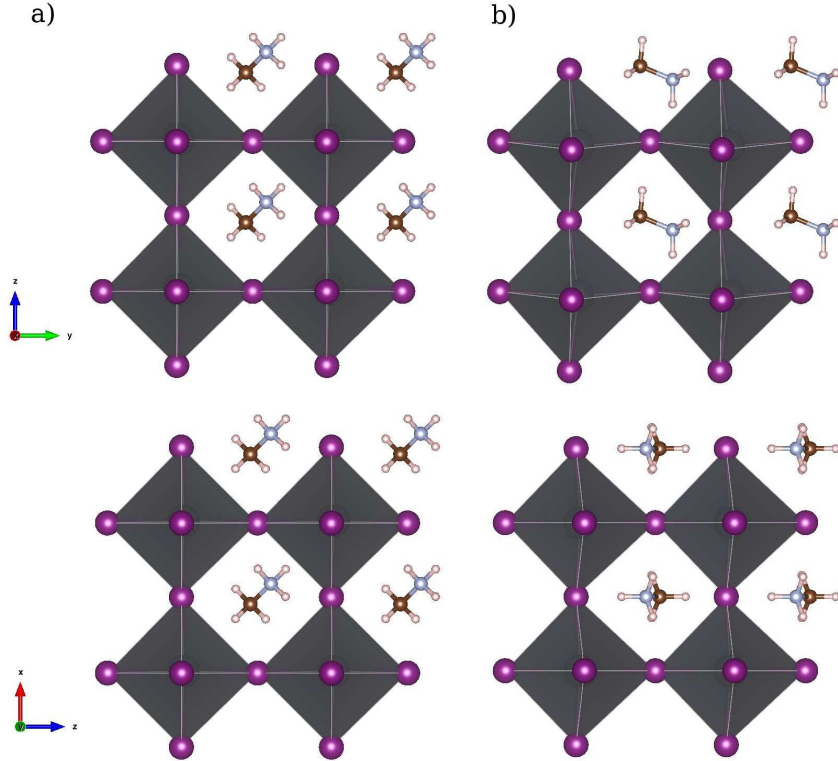


FIG. 1. Relaxed structures of the cubic phase of $\text{CH}_3\text{NH}_3\text{PbI}_3$ for two different orientations of the cations, namely along (a) (111) and (b) (011) (b). The views along the xy and xz planes are shown in the upper and lower panels, respectively.

orientations the energy gap computed without SOC lies in the 1.5-1.7 eV range, close to the experimental value of about 1.55 eV^{22,28}. However, as already shown⁵, this agreement is due to a fortuitous cancellation of errors, namely the GGA underestimates the bandgap, but this is counterbalanced by the lack of spin-orbit interaction. It is well known that the bottom of the conduction band mainly originates from the p orbitals of Pb, while the top of the valence band is derived from the p orbitals of I. The highest occupied molecular orbital (HOMO) of methylammonium is found deep below the valence band, approximately 5 eV below the valence band maximum (VBM). Thus, one may argue that CH_3NH_3 does not play any role in the optical and electronic response of such materials, but that rather it does only contribute to their structural cohesion. However, a careful analysis of the density of states (DOS) projected on the various atoms [see Fig. 3(a) and Supplementary Figure 3] reveals that there is a small contribution ~ 0.5 eV below the VBM attributable to the organic molecules. This indicates that indeed there is interaction between CH_3NH_3 and the

inorganic PbI_6 octahedra, in the form of hydrogen bonds between N and I.

A closer inspection to the bandstructures reveals that the orientation of CH_3NH_3 has a profound impact on the nature of the bandgap. In fact, while for the (111) case the gap is direct at the R point, the cationic rotation induces a transition to an indirect gap, and when MA is along (011) the conduction band minimum (CBM) shifts along the $\text{R} \rightarrow \Gamma$ line. Accordingly, the vertical energy difference between the CBM and the conduction band energy at R is 25 meV, as shown in the inset of Fig. 2(b). The effect persists when SOC is turned on, as shown in Fig. 2(c) and Fig. 2(d). In this case, a slight shift of the VBM towards Γ occurs as well, reducing the CB vertical energy difference approximately to half the non-SOC value. We stress here that the (011) orientation is not a special case: the indirect bandgap does appear for all the equivalent orientations, namely (0 ± 11) , (01 ± 1) , (± 101) , (± 110) , (10 ± 1) , (01 ± 1) . As an example, in Supplementary Figure 4 we show the (0-11) case, for which the CBM shifts in the direction opposite to that shown in Fig. 2, namely $\text{R} \rightarrow \text{M}$.

Such gap transformation is the most remarkable result of the interaction between the organic molecules and the inorganic framework, which is driven by the dispersive forces. As a result, CH_3NH_3 exerts strain on the PbI_6 octahedra and changes the nature of the bandgap. This is unusual in the perovskites world and it is a unique peculiarity of such hybrid systems. Typical inorganic perovskites such as SrTiO_3 respond to very small uniaxial strains, as those induced by the antiferrodistortive phase transition, by splitting their 3-fold degenerate CBM²⁹. To the best of our knowledge very few semiconductors see their bandgap changing from direct to indirect under the effect of strain. An example is given by layered transition metals chalcogenides, like for instance MoSe_2 single-layer, where the gap change is attributed to phonon softening³⁰. Intriguingly also for $\text{CH}_3\text{NH}_3\text{PbI}_3$ we observe some softening of our calculated low-energy optical phonon modes, when the methylammonium molecule rotates along the (011) directions. In particular the calculated energy red shift is of the order of 10 cm^{-1} (see Supplementary Figure 7).

We have carefully verified that the indirect bandgap is not an artifact of our computation method. Firstly, we analyzed the relaxation in a $2\times 2\times 2$ (96 atoms) supercell to establish whether further low-symmetry configurations are possible. The supercell converged geometries are very similar to the unit cell geometries repeated in space due to periodic boundary conditions. The calculations reveal no particular changes, although the size of the supercell

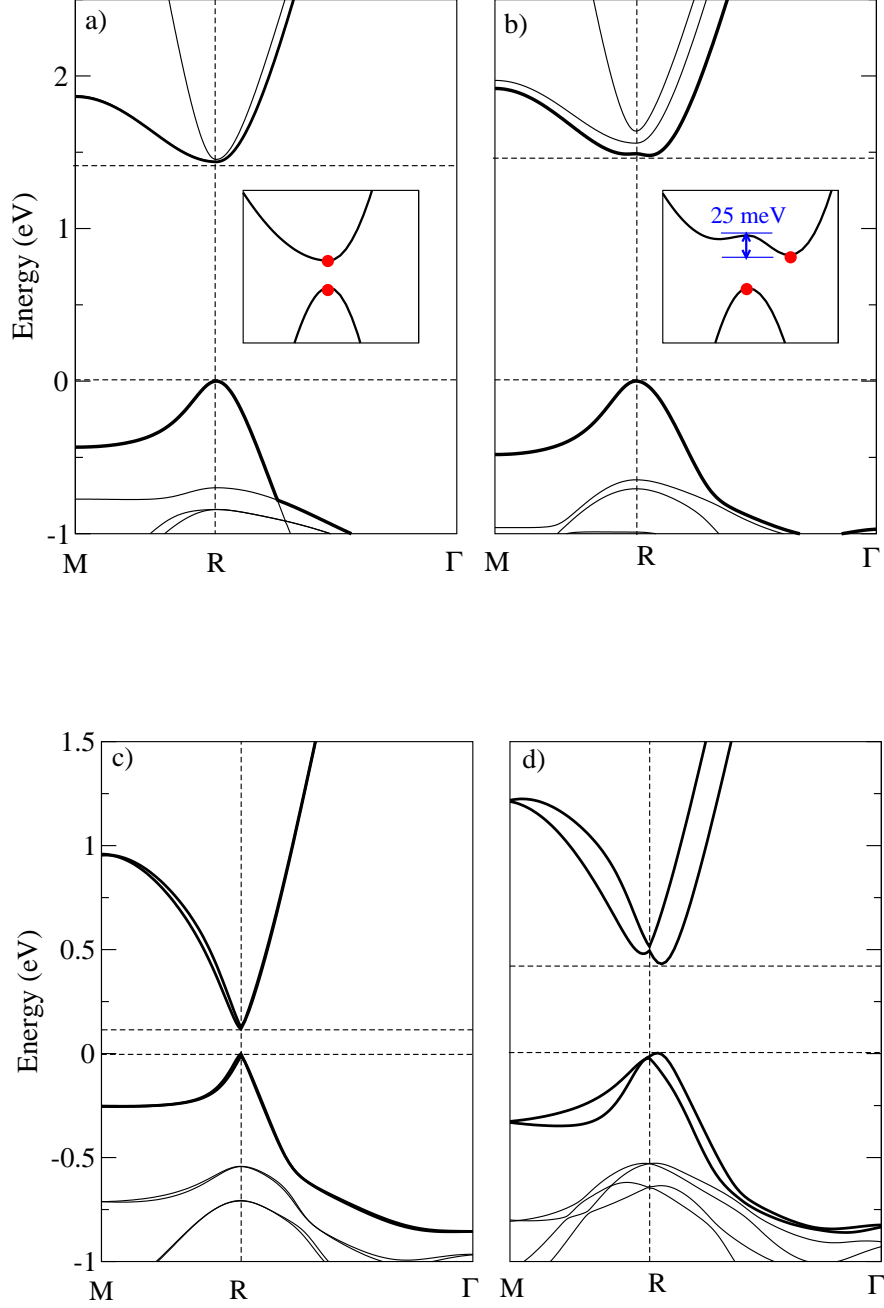


FIG. 2. Band structure of the fully relaxed $\text{CH}_3\text{NH}_3\text{PbI}_3$ crystal for molecule orientation along (111), (a) and (011) (b). The insets show a magnification of the bands (which have been shifted in energy for convenience) around the bandgap and highlight the changes in the VBM and CBM caused by the rotation of CH_3NH_3 . Note that for the (011) orientation the bandgap becomes indirect. The relativistic SOC bandstructures are shown in panels (c) and (d) for (111) and (011).

would allow the PbI_6 octahedra to rotate or tilt. Consequently, the features of the bandgaps are preserved both at the qualitative as well as the quantitative level.

Secondly, we have tested different vdW functionals by comparing the geometries obtained with the Tkatchenko-Scheffler (TS) scheme²⁴ to those calculated with the empirical Grimme’s method³¹ and with a recently developed sophisticated many-body dispersion (MBD) correction³². As shown in Supplementary Figure 1, the unit cell volume compares well with the experimental value for all the vdW-corrected functionals, although that calculated with the TS scheme is closer. Thus, in general, the TS and Grimme’s pairwise dispersion methods provide a sufficiently good description of our system as found in a recent work on molecular crystals¹⁷. In any case the indirect bandgap is found for all the calculated geometries, including those obtained with the MBD correction. In contrast, when dispersion interactions are not included the gap remains direct since the structure does not present enough distortion. Then, we have performed calculations using the HSE06³³ screened hybrid functional by starting from the optimal relaxed structures. Also in this case the bandgap remains indirect (see Supplementary Figure 3), although the overall energy distance between the CBM and the VBM increases, as expected.

Finally, we have performed additional calculations to establish whether or not the observed effect is the result of the interaction of the MA dipole with its periodic images. We have then verified that the position of the VBM and the CBM does not shift (i) upon flipping the molecule’s dipole moment, and (ii) upon applying a rigid rotation of the molecule from the 111 to the 110 orientation (Supplementary Figure 5). This confirms that it is the distortion of the inorganic PbI_6 octahedra to govern the shape of the CBM and VBM and not the dipole moment of the organic molecule.

As a last element of our analysis we have investigated the relative stability of the different molecular orientations. In particular, we have performed nudged elastic band calculations and evaluated the barrier height for a MA rotation from (011) to (111), taking into account possible changes in the cell geometry and the lattice vectors. We have found a barrier of 20 meV (1.929 kJ/mol), which is less than $k_{\text{B}}T$, and it is similar to values found recently in literature³⁴. This confirms the concept that above room temperature the molecules rotate at all time. Given the strong dependence of the position in k -space of the CBM and the VBM on the cell geometry, the fast molecular rotation implies that the nature and shape of the bandgap are rapidly-varying functions of time. Recently Mosconi et al.³⁵ published

Car-Parinello molecular dynamics simulations for a $2 \times 2 \times 2$ $\text{CH}_3\text{NH}_3\text{PBI}_3$ supercell at 319K, showing fluctuations of ± 0.1 - 0.2 eV in the position of the VBM, and thus giving evidence that the size of the bandgap changes as function of the MA rotation. Here we do a step forward and demonstrate that for some molecular orientations the bandgap turns from direct to indirect.

Optical absorption

In order to seek further evidence of the presence of the indirect bandgap, we have calculated the perovskite’s optical absorption and compared it with available experimental data. The calculations have been performed over the electronic structure obtained with the GGA including vdW interaction in the independent particle approximation and without SOC. Although the fortuitous cancellation of errors returns a bandgap close to experiments, we concentrate here on the shape of the spectrum around the absorption edge. The calculations are performed for the two orientations of the CH_3NH_3 molecule, and the spectra are presented in Fig. 3(c).

When methylammonium is aligned along the (111) direction the bandgap is direct and measures $1.423 \text{ eV} = 871 \text{ nm}$. The absorption profile then increases monotonically from that value, indicating the possibility of direct transitions across the band edges. In contrast, when CH_3NH_3 is placed along (011) the bandgap is indirect, and in general slightly larger than that corresponding to the (111) orientation. In particular, for (011) we find a direct gap of $1.611 \text{ eV} = 769 \text{ nm}$ and an indirect one of $1.629 \text{ eV} = 761 \text{ nm}$. Here, the shape of the absorption spectrum is quite different from the (111) case. We note a “two-step” absorption profile [see the inset of Fig. 3(c)], with a small absorption amplitude developing at the band edge followed by a significantly more pronounced increase at around 750 nm. This reflects the indirect nature of the bandgap and the fact that indirect transitions are not allowed, unless assisted by phonons. Certainly, the level of theory used here is not complete and one should use many-body methods for deriving a more qualitative picture³⁶, however the inclusion of excitonic effects is not necessary to make our main point about the shape of the spectrum around the absorption edge. In fact the differences between the direct and indirect bandgap are very evident from the inset of Fig. 3(c), and should be compared with the typical experimental absorption spectrum measured at 300 K given

in Supplementary Figure 6. This latter features a small amplitude around the bandgap followed by a rapid increase after about 50 nm, which seems to be a robust feature in the experimentally measured spectra, regardless of the morphology of the material^{7,22,37} and resistant to film quality degradation³⁸.

Whether or not such near-edge feature can be attributed to the indirect bandgap is however difficult to establish with certainty. In fact, at 300 K the MAs are free to rotate and sample the many quasi-equivalent (011) and (111) orientations. Thus, it is expected that no sharp indirect bandgap can be observed, but rather a smooth absorption spectra starting around the average bandgap value. Interestingly, we point out that our finding could help explaining the recently observed line broadening in photoluminescence experiments³⁹, attributed to coupling with phonons. In fact, low energy phonons are associated with cation rotations, which in turn would shift the CBM to different positions. As a result, the range of optical gap would change as function of temperature thus broadening the emission spectrum. Measurement of the optical absorption and thermal characteristics using very high sensitivity techniques such as photothermal deflection spectroscopy might reveal the existence of the indirect bandgap by fine lowering of temperature below 300 K thus freezing the MA (011)-like orientations.

DISCUSSION

Absorbing light efficiently and transporting the photocurrent with some gained voltage are the most important aspects in the design of a solar cell. The two processes can be characterised, respectively, by an empirical absorption length, L_α , inversely proportional to the absorption^{40,41}, and by the carrier diffusion length, L_{diff} . This is a measure of the mean distance travelled by carriers before recombining⁴²⁻⁴⁴, it is directly proportional to the carrier lifetime, τ , and it depends on several factors (mobility, carrier concentration, etc.). In solar cells it is essential to fulfil the condition $r = L_{\text{diff}}/L_\alpha > 1$ to ensure that the photogenerated carriers can be extracted and collected. For practical reasons $r \gg 1$ is required for high power conversion efficiency.^{40-42,45}

In general, direct bandgap semiconductors, such as GaAs, have strong absorption and thus short L_α , but this comes with fast carrier recombination and hence relatively small L_{diff} . The situation is opposite when the bandgap is indirect (e.g. in Si). An ideal balance

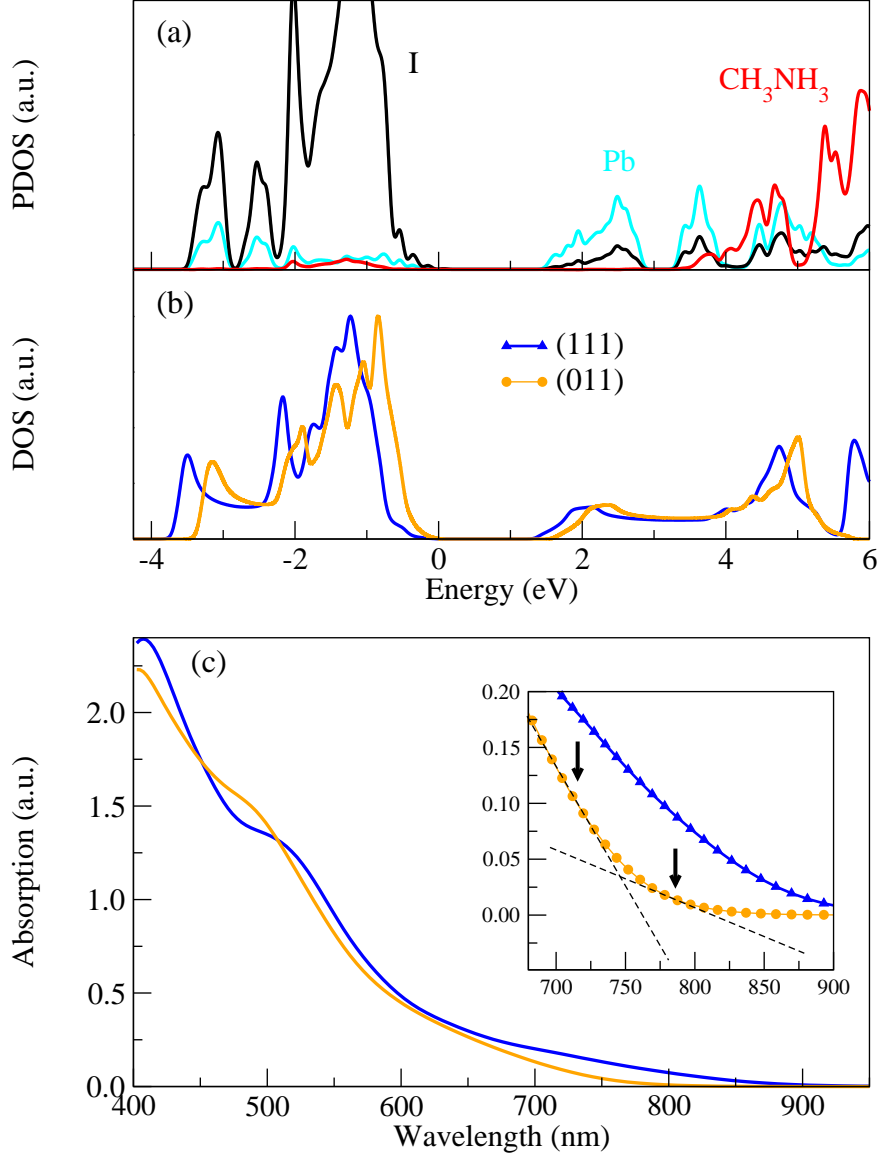


FIG. 3. Electronic and optical properties of the cubic phase $\text{CH}_3\text{NH}_3\text{PbI}_3$. In panel (a) we present the projected density of states for the case of the (111) oriented molecule on the Pb (cyan), I (black) species and the CH_3NH_3 (red). In panel (b) we display the density of states as a function of the chemical potential for the molecule oriented along the (111) and (011) directions. In panel (c) the calculated absorption spectra are plotted for the different orientation of CH_3NH_3 clearly showing the impact the organic cation rotation. The inset in (c) is a magnification of the same quantity around the low-energy region.

between L_α and L_{diff} is present in some indirect bandgap semiconductors such as Cu_3N ^{41,42}, where the direct transition starts a few $k_B T$ above the indirect gap, yielding a short L_α . The small difference between the indirect gap and the lowest direct transition ensures that the absorption is not greatly affected by the indirect gap till the direct transitions start to dominate the absorption spectrum. In contrast, the lifetime of the photogenerated carriers, which relax to the band edges in the indirect gap semiconductors, is longer than that of the direct ones by orders of magnitudes⁴³ ensuring a large L_{diff} . This class of indirect semiconductors promises remarkable improvement in efficiency via the large L_{diff}/L_α ratio^{41,42}.

From this short discussion and our results at hand we can speculate on the possible origin of the high efficiency in hybrid perovskites solar cells. Our calculations establish that, under certain conditions of molecule alignment, the bandgap of the high-temperature phase of $\text{CH}_3\text{NH}_3\text{PbI}_3$ can be indirect and not always direct as previously believed. This feature originates from the strain exerted on the PbI_6 octahedra by the organic molecules, when these points mostly toward one of the unit cell faces rather than along the diagonal, which constitute shallow minima in the total energy profile. The indirect bandgap is tens of meV smaller than the direct one and the position of the CBM with respect to the VBM depends on the specific orientation of the molecules. This analysis delivers a picture of $\text{CH}_3\text{NH}_3\text{PbI}_3$ as a “dynamical” bandgap semiconductor, where the term “dynamical” refers to the fact that the position in k -space of the CBM depends on the molecular alignment, which in turn fluctuates at room temperature. The calculated absorption spectrum near the band edge, characterized by a shallow amplitude at about 800 nm followed by a rapid enhancement within 50 nm, is very similar for (011) and equivalent orientations of the molecules, indicating that it is a feature robust to the molecular rotation and disorder.

The presence of an indirect bandgap, with only a small displacement in k -space with respect to the direct point, suggests that the rapid relaxation of the photo-excited electrons to the conduction band minimum is still possible. This process is incoherent, mediated by acoustic phonons, and spontaneously breaks the excitons in free carriers. As a second effect of the collapse of the electrons to the indirect conduction band minimum is that the lifetime of the minority carriers is enhanced, so that radiative recombination is partially suppressed. Such suppression is not complete since experiments reveal luminescence, however it contributes to prolong the carrier lifetime. In fact, it is interesting to note that experiments report that the luminescence gets suppressed as the material crystallizes³⁷ and that in any

case it is sensitive to the sample morphology and quality⁴⁶. Considering that the crystallization process leads to the geometries described here, such suppression of the luminescence upon ordering supports our argument. To complete the picture it is also worth reminding that the absence of strong scattering centers inhibits incoherent recombination, so that L_{diff} remains long⁴⁷.

CONCLUSIONS

Despite the tremendous advances in studying and understanding hybrid perovskites from both the theoretical and the experimental point of views, yet the reason behind the extended carrier lifetime in these materials remains a mystery. Our work suggests that extended carrier lifetimes in $\text{CH}_3\text{NH}_3\text{PbI}_3$ might be a consequence of the “dynamical” position of the conduction band minimum forming a basin around a high symmetry point in the k -space. This proposed dynamical bandgap, induced by the molecular motion, prohibits carrier recombination, favors exciton separation thus increasing the conversion efficiency of the photovoltaic absorber $\text{CH}_3\text{NH}_3\text{PbI}_3$. Crucially, all such phenomenology appears to be initiated by the geometry assumed by the molecules following full geometry relaxation. A set of differently oriented CH_3NH_3 cation geometries, relaxed without any symmetry constraints using DFT including van der Waals forces, lead to geometries where the PbI_6 octahedra distort. The band-structure corresponding to such geometries present an indirect bandgap, which persists upon bandgap corrections via screened hybrid functionals and spin-orbit coupling. Finally, we propose that a possible way for engineering the efficiency of hybrid perovskites is to induce distortion to the PbI_6 octahedra either by using strain or organic molecules strongly interacting with the inorganic cages.

COMPUTATIONAL DETAILS

DFT calculations

The electronic properties of the hybrid perovskites have been calculated with the all-electron FHI-AIMS code at the level of GGA in the Perdew-Burke-Ernzerhof (PBE)²³ parameterization. Long-range van der Waals interactions have been taken into account via the Tkatchenko and Scheffler (TS) scheme²⁴, which is also constructed over a GGA and a pairwise dispersive

potential. The reciprocal space integration was performed over an $8\times 8\times 8$ Monkhorst-Pack grid⁴⁸. A pre-constructed high-accuracy all-electron basis set of numerical atomic orbitals was employed, as provided by the FHI-AIMS “tight” default option (more details are given in Supplementary Information). Unconstrained structural optimization was performed with the Broyden-Fletcher-Goldfarb-Shanno algorithm⁴⁹ with a tolerance of 10^{-3} eV/Å .

Additional calculations, in particular concerning the use of the hybrid functional HSE06³³, were performed using the GAUSSIAN suite⁵⁰, with the periodic boundary condition⁵¹ code version. The Def2-⁵² series of GAUSSIAN basis sets were optimized following our own procedure, described in Ref. [53], for the atomic species of interest in this work. Most numerical settings in GAUSSIAN were left at the default values, *e.g.*, unconstrained geometry optimization settings, integral cut-offs, and self-consistent convergence thresholds. The standard rms force threshold in GAUSSIAN for geometry optimizations is 450×10^{-6} hartrees/bohr. The default k -point mesh of $8\times 8\times 8$ was used for the 12 atoms unit cell of $\text{CH}_3\text{NH}_3\text{PbI}_3$.

Finally calculations involving the spin-orbit interaction have been carried out using the Vienna ab initio simulation package (VASP). A plane wave basis set energy cutoff of 520 eV was considered in the calculations and Brillouin zone integration was performed using $8\times 8\times 8$ k -point mesh centered at the Gamma point. Dispersion correction to the PBE was done within the method of Tkatchenko and Scheffler (DFT-TS) —recently implemented in the 5.3.5 version of VASP — used to account for Van der Waals interactions. The projector augmented wave (PAW) pseudopotentials were used for all elements $5d^{10}6s^26p^2$ valence electron potential was used for the Pb atom.

The linear optical absorption has been obtained with FHI-AIMS by computing the momentum matrix elements in a 5 eV energy window around the Fermi level and then by using the Fermi golden rule approximation. A dense k -point sampling of $15\times 15\times 15$ has been employed to ensure converged spectra.

Phonon calculations

Phonons spectra were computed with the frozen-phonon approach for a fully relaxed $2\times 2\times 2$ supercells using the Phonopy⁵⁴ code in combination with FHI-AIMS A displacement of 0.001 Å was applied to each atom in the three space directions to compute the dynamical matrix. The phonon density of states used the Γ point sampling while the full phonon band structure

was generated using the Γ , M , X and R high symmetry points in the Brillouin zone.

* mottac@tcd.ie

† felmellouhi@qf.org.qa

- ¹ Snaith, H. J. Perovskites: The emergence of a new era for low-cost, high-efficiency solar cells. *J. Phys. Chem. Lett.* **4**, 3623–3630 (2013).
- ² Boix, P. P., Nonomura, K., Mathews, N. & Mhaisalkar, S. G. Current progress and future perspectives for organic/inorganic perovskite solar cells. *Mater. Today* **17**, 16–23 (2014).
- ³ Loi, M. A. & Hummelen, J. C. Hybrid solar cells: Perovskites under the sun. *Nat. Mater.* **12**, 1087–1089 (2013).
- ⁴ Deschler, F. *et al.* High photoluminescence efficiency and optically pumped lasing in solution-processed mixed halide perovskite semiconductors. *J. Phys. Chem. Lett.* 1421–1426 (2014).
- ⁵ Mosconi, E., Amat, A., Nazeeruddin, M. K., Grätzel, M. & De Angelis, F. First-principles modeling of mixed halide organometal perovskites for photovoltaic applications. *J. Phys. Chem. C* **117**, 13902–13913 (2013).
- ⁶ Liu, M., Johnston, M. B. & Snaith, H. J. Efficient planar heterojunction perovskite solar cells by vapour deposition. *Nature* **501**, 395–398 (2013).
- ⁷ Xing, G. *et al.* Long-range balanced electron- and hole-transport lengths in organic-inorganic $\text{CH}_3\text{NH}_3\text{PbI}_3$. *Science* **342** (2013).
- ⁸ Yin, W.-J., Shi, T. & Yan, Y. Unusual defect physics in $\text{CH}_3\text{NH}_3\text{PbI}_3$ perovskite solar cell absorber. *Appl. Phys. Lett.* **104**, – (2014).
- ⁹ Kim, J., Lee, S.-H., Lee, J. H. & Hong, K.-H. The role of intrinsic defects in methylammonium lead iodide perovskite. *J. Phys. Chem. Lett.* 1312–1317 (2014).
- ¹⁰ Brivio, F., Butler, K. T., Walsh, A. & van Schilfhaarde, M. Relativistic quasiparticle self-consistent electronic structure of hybrid halide perovskite photovoltaic absorbers. *Phys. Rev. B* **89**, 155204 (2014).
- ¹¹ Umari, P., Mosconi, E. & De Angelis, F. Relativistic gw calculations on $\text{CH}_3\text{NH}_3\text{PbI}_3$ and $\text{CH}_3\text{NH}_3\text{SnI}_3$ perovskites for solar cell applications. *Sci. Rep.* **4** (2014).
- ¹² Baikie, T. *et al.* Synthesis and crystal chemistry of the hybrid perovskite $(\text{CH}_3\text{NH}_3)\text{PbI}_3$ for solid-state sensitised solar cell applications. *J. Mater. Chem. A* **1**, 5628–5641 (2013).

- ¹³ Knop, O., Wasylshen, R. E., White, M. A., Cameron, T. S. & Oort, M. J. M. V. Alkylammonium lead halides. part 2. $\text{CH}_3\text{NH}_3\text{PbX}_3$ ($\text{X}=\text{Cl}, \text{Br}, \text{I}$) perovskites: cuboctahedral halide cages with isotropic cation reorientation. *Can. J. Chem.* **68**, 412–422 (1990).
- ¹⁴ Wang, Y. *et al.* Density functional theory analysis of structural and electronic properties of orthorhombic perovskite $\text{CH}_3\text{NH}_3\text{PbI}_3$. *Phys. Chem. Chem. Phys.* **16**, 1424–1429 (2014).
- ¹⁵ Menéndez-Proupin, E., Palacios, P., Wahnón, P. & Conesa, J. C. Self-consistent relativistic band structure of the $\text{CH}_3\text{NH}_3\text{PbI}_3$ perovskite. *Phys. Rev. B* **90**, 045207 (2014). URL <http://link.aps.org/doi/10.1103/PhysRevB.90.045207>.
- ¹⁶ Egger, D. A. & Kronik, L. Role of dispersive interactions in determining structural properties of organic–inorganic halide perovskites: Insights from first-principles calculations. *J. Phys. Chem. Lett.* **5**, 2728–2733 (2014).
- ¹⁷ Kronik, L. & Tkatchenko, A. Understanding molecular crystals with dispersion-inclusive density functional theory: Pairwise corrections and beyond. *Acc. Chem. Res.* (2014).
- ¹⁸ Even, J., Pedesseau, L., Jancu, J.-M. & Katan, C. Importance of spinorbit coupling in hybrid organic/inorganic perovskites for photovoltaic applications. *J. Phys. Chem. Lett.* **4**, 2999–3005 (2013).
- ¹⁹ Even, J., Pedesseau, L., Jancu, J.-M. & Katan, C. DFT and KP modelling of the phase transitions of lead and tin halide perovskites for photovoltaic cells. *physica status solidi (RRL) Rapid Research Letters* **8**, 31–35 (2014).
- ²⁰ Feng, J. & Xiao, B. Crystal structures, optical properties, and effective mass tensors of $\text{CH}_3\text{NH}_3\text{PbX}_3$ ($\text{X} = \text{I}$ and Br) phases predicted from HSE06. *J. Phys. Chem. Lett.* **5**, 1278–1282 (2014).
- ²¹ Giorgi, G., Fujisawa, J.-I., Segawa, H. & Yamashita, K. Cation role in structural and electronic properties of 3d organic-inorganic halide perovskites: A DFT analysis. *J. Phys. Chem. C* **118**, 12176–12183 (2014).
- ²² Lee, M. M., Teuscher, J., Miyasaka, T., Murakami, T. N. & Snaith, H. J. Efficient hybrid solar cells based on meso-superstructured organometal halide perovskites. *Science* **338**, 643–647 (2012).
- ²³ Perdew, J. P., Burke, K. & Ernzerhof, M. Generalized gradient approximation made simple. *Phys. Rev. Lett.* **77**, 3865–3868 (1996).
- ²⁴ Tkatchenko, A. & Scheffler, M. Accurate molecular van der waals interactions from ground-state

- electron density and free-atom reference data. *Phys. Rev. Lett.* **102**, 073005 (2009).
- ²⁵ Poglitsch, A. & Weber, D. Dynamic disorder in methylammoniumtrihalogenoplumbates (ii) observed by millimeter-wave spectroscopy. *J. Chem. Phys.* **87**, 6373 (1987).
- ²⁶ Brivio, F., Walker, A. B. & Walsh, A. Structural and electronic properties of hybrid perovskites for high-efficiency thin-film photovoltaics from first-principles. *APL Materials* **1**, – (2013).
- ²⁷ Stoumpos, C. C., Malliakas, C. D. & Kanatzidis, M. G. Semiconducting tin and lead iodide perovskites with organic cations: phase transitions, high mobilities, and near-infrared photoluminescent properties. *Inorg. Chem.* **52**, 9019–9038 (2013).
- ²⁸ Kojima, A., Teshima, K., Shirai, Y. & Miyasaka, T. Organometal halide perovskites as visible-light sensitizers for photovoltaic cells. *J. Am. Chem. Soc.* **131**, 6050–6051 (2009).
- ²⁹ El-Mellouhi, F., Brothers, E. N., Lucero, M. J., Bulik, I. W. & Scuseria, G. E. Structural phase transitions of the metal oxide perovskites SrTiO₃, LaAlO₃, and LaTiO₃ studied with a screened hybrid functional. *Phys. Rev. B* **87**, 035107 (2013).
- ³⁰ Horzum, S. *et al.* Phonon softening and direct to indirect band gap crossover in strained single-layer MoSe₂. *Phys. Rev. B* **87**, 125415 (2013).
- ³¹ Grimme, S. Semiempirical GGA-type density functional constructed with a long-range dispersion correction. *J. Comput. Chem.* **27**, 1787–1799 (2006).
- ³² Tkatchenko, A., DiStasio, R. A., Car, R. & Scheffler, M. Accurate and efficient method for many-body van der Waals interactions. *Phys. Rev. Lett.* **108**, 236402 (2012).
- ³³ Krukau, A. V., Vydrov, O. A., Izmaylov, A. F. & Scuseria, G. E. Influence of the exchange screening parameter on the performance of screened hybrid functionals. *J. Chem. Phys.* **125** (2006).
- ³⁴ Frost, J. M. *et al.* Atomistic origins of high-performance in hybrid halide perovskite solar cells. *Nano Lett.* **14**, 2584–2590 (2014).
- ³⁵ Mosconi, E., Quarti, C., Ivanovska, T., Ruani, G. & De Angelis, F. Structural and electronic properties of organo-halide lead perovskites: a combined IR-spectroscopy and ab initio molecular dynamics investigation. *Phys. Chem. Chem. Phys.* (2014).
- ³⁶ Even, J., Pedesseau, L. & Katan, C. Analysis of multivalley and multibandgap absorption and enhancement of free carriers related to exciton screening in hybrid perovskites. *J. Phys. Chem. C* **118**, 11566–11572 (2014).
- ³⁷ Burschka, J. *et al.* Sequential deposition as a route to high-performance perovskite-sensitized

- solar cells. *Nature* **499**, 316–319 (2013).
- ³⁸ Niu, G. *et al.* Study on the stability of $\text{CH}_3\text{NH}_3\text{PbI}_3$ films and the effect of post-modification by aluminum oxide in all-solid-state hybrid solar cells. *J. Mater. Chem. A* **2**, 705–710 (2014).
- ³⁹ Wehrenfennig, C., Liu, M., Snaith, H. J., Johnston, M. B. & Herz, L. M. Homogeneous emission line broadening in the organo lead halide perovskite $\text{CH}_3\text{NH}_3\text{PbI}_3\text{XCl}_x$. *J. Phys. Chem. Lett.* **5**, 1300–1306 (2014).
- ⁴⁰ Loferski, J. J. Theoretical considerations governing the choice of the optimum semiconductor for photovoltaic solar energy conversion. *Journal of Applied Physics* **27**, 777–784 (1956).
- ⁴¹ Alharbi, F. *et al.* Abundant non-toxic materials for thin film solar cells: Alternative to conventional materials. *Renew. Energ.* **36**, 2753 – 2758 (2011).
- ⁴² Zakutayev, A. *et al.* Defect tolerant semiconductors for solar energy conversion. *J. Phys. Chem. Lett.* **5**, 1117–1125 (2014).
- ⁴³ Fonash, S. *Solar Cell Device Physics* (Oxford: Academic Press, 2010).
- ⁴⁴ Law, M., Solley, E., Liang, M. & Burk, D. Self-consistent model of minority-carrier lifetime, diffusion length, and mobility. *Electron Device Lett.* **12**, 401–403 (1991).
- ⁴⁵ Grätzel, M. Photoelectrochemical cells. *Nature* **414**, 338–344 (2001).
- ⁴⁶ Choi, J. J., Yang, X., Norman, Z. M., Billinge, S. J. L. & Owen, J. S. Structure of methylammonium lead iodide within mesoporous titanium dioxide: Active material in high-performance perovskite solar cells. *Nano Lett.* **14**, 127–133 (2013).
- ⁴⁷ Stranks, S. D. *et al.* Electron-hole diffusion lengths exceeding 1 micrometer in an organometal trihalide perovskite absorber. *Science* **342**, 341–344 (2013).
- ⁴⁸ Monkhorst, H. J. & Pack, J. D. Special points for brillouin-zone integrations. *Phys. Rev. B* **13**, 5188–5192 (1976).
- ⁴⁹ Press, W. H., Teukolsky, S. A., Vetterling, W. T. & Flannery, B. P. *Numerical recipes* (Cambridge University Press, 1997), 3 edn.
- ⁵⁰ Frisch, M. J. *et al.* Gaussian 09 revision {B}.01. Gaussian Inc. Wallingford CT 2009.
- ⁵¹ Kudin, K. N. & Scuseria, G. E. Linear-scaling density-functional theory with gaussian orbitals and periodic boundary conditions: Efficient evaluation of energy and forces via the fast multipole method. *Phys. Rev. B* **61**, 16440–16453 (2000).
- ⁵² Weigend, F. & Ahlrichs, R. Balanced basis sets of split valence, triple zeta valence and quadruple zeta valence quality for H to Rn: Design and assessment of accuracy. *Phys. Chem. Chem. Phys.*

7, 3297–3305 (2005).

- ⁵³ El-Mellouhi, F., Brothers, E. N., Lucero, M. J. & Scuseria, G. E. Modeling of the cubic and antiferrodistortive phases of SrTiO₃ with screened hybrid density functional theory. *Phys. Rev. B* **84**, 115122 (2011).
- ⁵⁴ Togo, A., Oba, F. & Tanaka, I. First-principles calculations of the ferroelastic transition between rutile-type and CaCl₂-type SiO₂ at high pressures. *Phys. Rev. B* **78**, 134106 (2008).

ACKNOWLEDGEMENTS

This work is sponsored by the European Research Council, QUEST project, (CM and SS) and by the Qatar Environment and Energy Research Institute (FE, FHAH, NT and SK). Computational resources have been provided by the supercomputer facilities at the Trinity Center for High Performance Computing, at ICHEC (project tcphy038b) and the research computing at Texas A&M University at Qatar. We acknowledge fruitful discussions with Simon Gelinias, Marcelo Carignano and Mohamed Lamine Madjet and thank Felix Deschler for sending his absorption spectra.

AUTHOR CONTRIBUTIONS

C.M. and F.E.M. contributed equally to the manuscript. C.M. and F.E.M. performed the computational research, C.M., F.E.M., S.K., N.T., F.A. and S.S. discussed the results. C.M., F.E.M. and S.S. contributed to the preparation of the manuscript.

ADDITIONAL INFORMATION

Competing financial interests: The authors declare no competing financial interests.